ELSEVIER
SAUNDERS

Neurol Clin 25 (2007) 947–973

NEUROLOGIC
CLINICS

Advanced MRI of Adult Brain Tumors

Geoffrey S. Young, MD[a,b,*]

[a]*Department of Radiology, Brigham and Women's Hospital, 75 Francis Street, Boston, MA 02115, USA*
[b]*Harvard Medical School, Boston, MA 02115, USA*

Over the last decade, advanced magnetic resonance (MR) techniques that produce image contrast reflecting attributes of tissue physiology and microstructure have begun to be widely applied in clinical brain tumor imaging at major academic centers. These techniques are all adapted from, and must be interpreted in the context of, conventional MRI techniques based on the fundamental physical properties of tissue protons—proton density, T1, T2, T2*, and delayed permeability—that produce image contrasts reflecting gross anatomy on a scale of 500 μm or greater.

This article introduces the preliminary clinical experience that guides the neurooncologic application of the most established of these techniques. Because the article is directed primarily at clinical neurologists and neurooncologists rather than neuroradiologists, the physical or physiologic principles underlying these techniques are not discussed in any detail, but the references for each section should provide an entry point to the more technical literature for the interested reader. Also, although the rapidly expanding literature describes dozens of advanced techniques currently under investigation, this discussion is limited to the most widely available, practical, and robust techniques: diffusion-weighted imaging (DWI), perfusion-weighted imaging MRI (PMR), dynamic contrast-enhanced T1 permeability imaging (T1P), diffusion-tensor imaging (DTI), and MR spectroscopy (MRS). It may help to note that PMR is also variously known as "perfusion-weighted imaging," "MR perfusion," "perfusion MR," and "dynamic susceptibility contrast imaging." T1P is also known as "dynamic contrast-enhanced imaging," among other terms. MRS is also known as "chemical shift imaging." The techniques themselves, the available hardware and software, and the clinical literature and practice are evolving so rapidly that this

* Department of Radiology, Brigham and Women's Hospital, 75 Francis St., Boston, MA 02115.
E-mail address: gsyoung@partners.org

doi:10.1016/j.ncl.2007.07.010

introduction will inevitably be out of date in important aspects even as this article goes to press.

Although qualitative interpretation of basic brain tumor MRI (including T2-weighted images and gadolinium [Gd]-enhanced T1-weighted images), remains the backbone of brain tumor imaging, in a significant number of cases, these techniques fail to allow confident and correct differential diagnosis, grading, and monitoring of brain tumor [1]. Thus, the immediate goals of tumor imaging include (1) initial differential diagnosis, to aid in the distinction of newly diagnosed brain tumors from non-neoplastic conditions such as tumefactive demyelination and ischemia and to aid in the differentiation of glioma from extra-axial neoplasm and metastasis; (2) preoperative therapeutic planning, to provide an estimate of tumor grade and to guide biopsy, resection, and local ablative therapy; and (3) therapeutic follow-up, to monitor disease progression and therapeutic response, including the differentiation of recurrent tumor from delayed radiation necrosis. These goals are related to but distinct from the scientific goals of advanced imaging that include a better understanding of the pathophysiology of brain tumor and improved prediction of therapeutic response.

Brain tumor cellularity: diffusion-weighted imaging

DWI contrast reflects the brownian motion of tissue water. Because the mean path length of water diffusion within each tissue voxel, characterized by the ''apparent diffusion coefficient'' (ADC), is determined by tissue barriers to diffusion on a scale of roughly 10 μm, the ADC in brain tissue is principally determined by tissue cellularity, as measured by the intracellular volume fraction and extracellular volume fractions [2,3].

Diffusion-weighted imaging differential diagnosis

DWI has a sensitivity and specificity of over 90% for distinguishing epidermoid (low ADC) from arachnoid cyst (high ADC) and distinguishing abscess (low ADC) from necrotic tumor (high ADC). The viscous keratin and cholesterol in epidermoid and the viscous and cellular pus in abscess produce a very low ADC that distinguishes these lesions from increased diffusivity in necrotic tumor and from normal or slightly low diffusivity in demyelinating plaque [4–7].

A low ADC in an intra-axial neoplasm should raise suspicion of lymphoma or metastasis, depending on the conventional MRI appearance, because the higher cellularity of these tumors generally produces an ADC that is significantly lower than that of glioma [8,9]. In an extra-axial lesion, meningioma and dural metastasis should be considered; however, although most gliomas have a much higher ADC (related to their lower cellularity), a number of case reports and several larger series have demonstrated a low ADC in a small number of glioblastomas (GBM). The resulting

significant overlap among ADC values in the three tumor types reinforces the need to integrate DWI with other advanced and conventional neuroimaging data for accurate clinical interpretation (Fig. 1) [8,10–12].

Diffusion-weighted imaging in preoperative grading and surgical planning

An inverse correlation between minimum ADC (ADC_{min}) and tumor cellularity has been verified by histology in a wide variety of tumors, including high- and low-grade glioma, lymphoma, medulloblastoma, meningioma, and metastases [8,13–17]. Within meningioma, a lower ADC has been demonstrated in atypical and malignant versus typical subtypes, but it is unfortunate that the overlap of the two groups precludes the use of the ADC for differentiation in individual patients [16]. In glioma, however, a number of groups have found that ADC_{min} values below a cutoff in the range of 1.7 to 2.5 can be used to distinguish high-grade glioma from low-grade glioma [18,19]. Again, overlap between tumor grades mandates that ADC_{min} information be combined with other advanced and conventional MRI data to reliably distinguish high-grade from low-grade glioma [9,18,20,21].

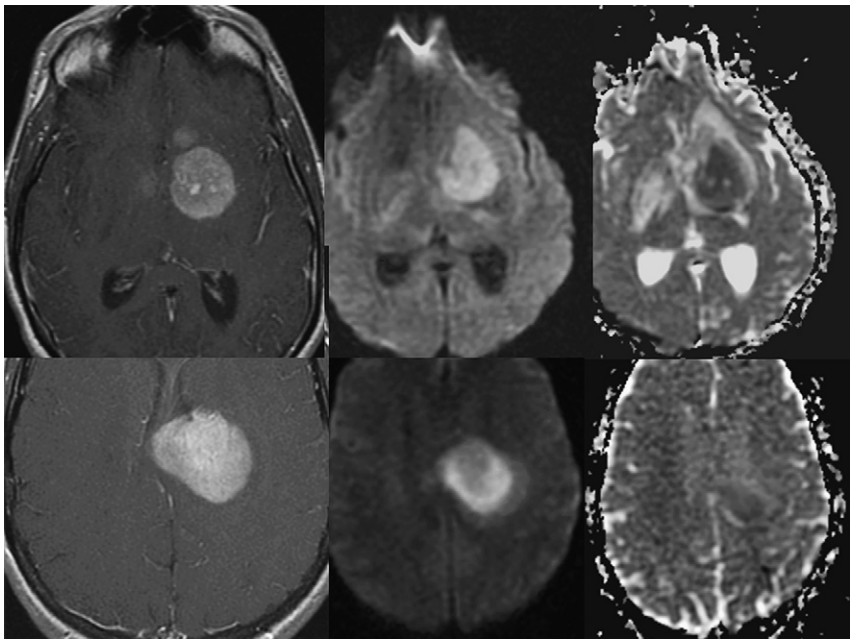

Fig. 1. T1 with contrast (*left*), DWI (*middle*), and apparent diffusion coefficient map (*right*) demonstrate markedly reduced diffusivity within a homogeneously enhancing periventricular lesion that extends across the corpus callosum (*top row*). Although this is strongly suggestive of primary central nervous system lymphoma, highly cellular GBM do occur (*bottom row*), so correlation with perfusion imaging is strongly indicated to assist in differential diagnosis.

Furthermore, ADC_{min} and tumor cellularity prove to be variable among tumors of a given grade, especially in high-grade glioma [22]. Although the presence of necrosis, hemorrhage, and calcification may contribute to the spread of the tumor ADC observed in each tumor grade, it seems likely that in large part, the heterogeneity of ADC_{min} within tumor grade reflects heterogeneity of cellularity among tumors of the same grade. This heterogeneity of cellularity within tumors of the same grade limits the utility of DWI as a surrogate for histopathology but raises the possibility that ADC_{min} could help to substratify tumors within grade, as suggested by a recent report stating that ADC estimates of cellularity accurately predict radiation responsiveness in glioma and metastasis [23].

Diffusion-weighted imaging monitoring of therapeutic response

On immediate postoperative MRI, ischemia at the margin of surgical resection or elsewhere [24] and pyogenic infection can produce a focally reduced ADC that is important to detect and can generally be distinguished from tumor based on the signal intensity on DWI, the morphology of the area, correlation with other pulse sequences, and correlation with history [25]. DWI may be very useful in following tumor treatment response and subsequent recurrence in individual patients because cytotoxic radiation and chemotherapy reduce tumor cellularity and thus increase the ADC within a given area of tumor [14,15,26–28]. The relative insensitivity of a glioma ADC to steroid therapy contrasts with a pronounced effect of steroids on enhancement, edema, and permeability and a debatable effect on blood volumes [29], suggesting that despite technical issues related to serial longitudinal registration of echoplanar data, DWI will remain valuable for tumor follow-up. A novel way of presenting longitudinal DWI follow-up data, called ''functional diffusion mapping,'' has recently received considerable attention, but it remains to be seen whether this method adds value compared with more straightforward methods of data presentation (Fig. 2) [30,31].

Tissue microstructural derangement: diffusion-tensor imaging

DTI is similar to DWI but involves the collection of additional data necessary to define the tensor (vector) describing the preferential direction and magnitude of water diffusion [32,33]. The degree to which water diffusion in tissue is facilitated in one direction and hindered in another—referred to as ''diffusion anisotropy''—is often characterized by a scalar value derived from the diffusion tensor: fractional anisotropy (FA).

Diffusion-tensor imaging in preoperative guidance

Because the myelin sheaths of white matter are one of the principal barriers to extracellular water diffusion in the brain, DTI allows a very sensitive

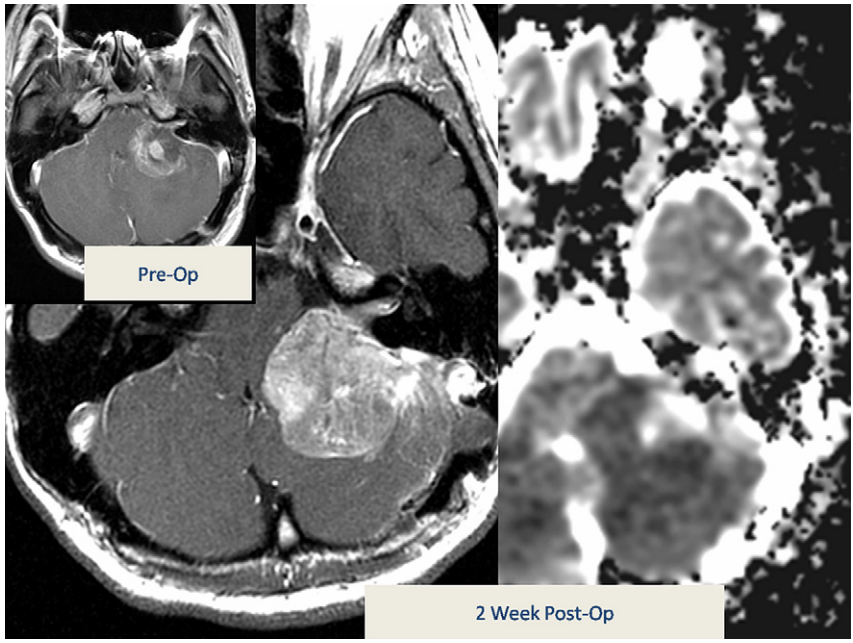

Fig. 2. Gd-enhanced T1-weighted images (*above left*) before and 2 weeks after surgical resection demonstrate surprisingly rapid increase in size of the enhancing mass. The very low diffusivity seen in the mass on the ADC map (*far right*) confirmed high cellularity of the lesion, consistent with rapid recurrence of medulloblastoma.

depiction of the orientation and integrity of white matter tracts. Various algorithms have been developed to trace white matter tracts by connecting the principal direction or directions of preferred diffusivity in each voxel to those of adjoining voxels. Especially when integrated with functional MRI, these tractography techniques have been used successfully to identify the location of eloquent white matter tracts displaced by tumor and to predict the degree of postoperative functional impairment based on intraoperative injury to these tracts [34–38].

Diffusion-tensor imaging in differential diagnosis

Although glioma cells infiltrate widely throughout the brain, anatomic MRI or positron emission tomography is not able to accurately characterize the extent of tumor infiltration beyond the area of abnormal T2 and cannot distinguish abnormal T2 related to infiltrative tumor from vasogenic edema. Because glioma infiltration disrupts the organization of the white matter tracts, FA and other anisotropy measures derived from DTI promise to allow definition of the degree of this tumor infiltration.

Some but not all recent studies have suggested that DTI can aid in the distinction of vasogenic edema surrounding metastases and meningioma

from nonenhancing tumor infiltration in glioma. The mixed success of the published reports suggests that the angular resolution, b-value, and signal-to-noise ratio achieved by a given DTI protocol will be critical determinants of the concentration of tumor that can be detected within white matter [39,40].

Diffusion-tensor imaging in glioma grading

Initial experience with DTI tractography revealed a continuous increase in organization of the white matter in proportion to the distance from the enhancing glioma core [34], but efforts to use DTI to define the margins of glioma white matter invasion have yielded mixed results [22,41–45]. Because white matter adjacent to glioma generally contains different proportions of vasogenic edema and tumor infiltration at different distances from the center of the tumor, it is difficult to define an unbiased region of interest for valid grouped data analysis. This difficulty is compounded by the challenge of obtaining a pathologic "gold standard," because extensive biopsy of grossly intact white matter around tumors is ethically unacceptable.

Diffusion-tensor imaging in tumor follow-up

Preliminary reports using FA in combination with ADC for differentiation of tumor recurrence from radiation necrosis have also been published, but the contribution of anisotropy measures remains to be fully defined [46]. Based on promising initial results in differentiating infiltrative tumor from vasogenic edema and in characterizing the extent of glioma white matter infiltration by FA, early reports of the development of a "fiber coherence index" and a number of other measures promise to allow more sensitive assessment of white matter microstructural disorganization than FA, by employing more sophisticated analyses of the directional information available from high-diffusion direction DTI (Fig. 3) [39,42,47–49].

Metabolite imaging in brain tumor: spectroscopy

MRS techniques essentially allow nuclear MR (NMR) spectroscopy to be performed in vivo, albeit at much lower field strength and sensitivity than in synthetic chemistry laboratory NMR scanners. As in NMR, proton MRS assays the number of each chemically distinct proton ($^1H_0$) species present in each voxel by detecting slight differences in the NMR frequency ("chemical shift") of each proton nucleus that result from shielding by the surrounding covalent bond electron cloud. The differences in proton resonance frequency are displayed on the x-axis of each spectrum (graph) in units of parts per million of the resonance frequency of a standard reference compound, rather than in hertz, to produce spectra that are

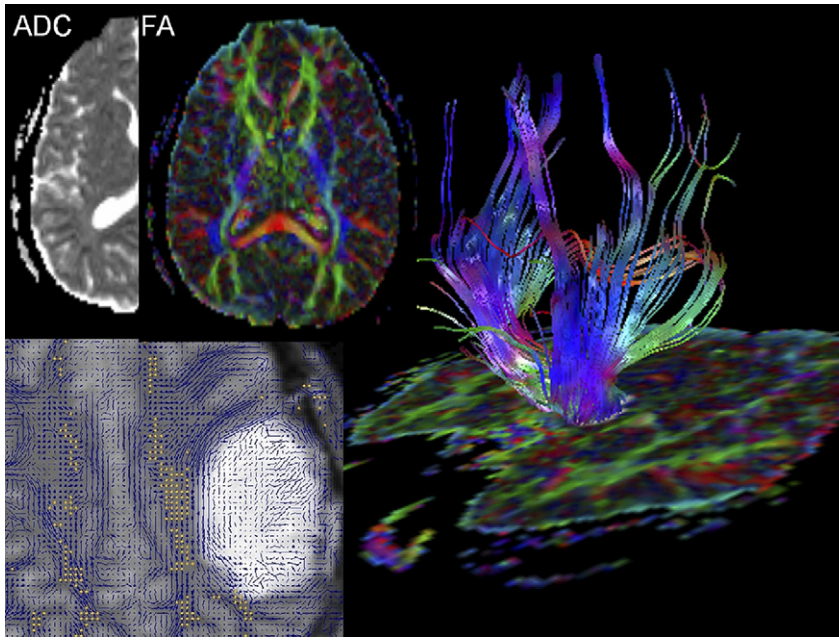

Fig. 3. FA color map and ADC maps (*upper left, as labeled*) from one subject demonstrate the dramatically increased sensitivity to the structure of myelinated white matter tracks obtained with DTI. Principal eigenvectors from diffusion-tensor tractography overlayed on anatomic MRI (*lower left*) from a different subject demonstrates displacement of white matter tracts by glioma. Tractogram from a third subject (*right*) illustrates the standard technique for displaying DTI data for surgical planning. (FA and tractogram images courtesy of Kelvin Wong, PhD, using Philips Pride Software at Jockey Club MRI Center, University of Hong Kong.)

comparable across field strengths. Because clinical MRS is not directly quantifiable, the y-axis of the graph represents arbitrary units of signal intensity scaled relative to the highest peak [50,51]. Simultaneous interrogation of two-dimensional (2D) or three-dimensional (3D) arrays of small voxels is referred to as 2D or 3D MR spectroscopic imaging (2D-MRSI or 3D-MRSI, respectively). 2D- or 3D-MRSI data can be used to produce impressive color ''metabolite maps'' that depict the spatial distribution of the different peak heights, areas, or peak ratios that can be derived from these spectra but are of limited use for clinical diagnosis because the primary data can only be assessed from the spectral graphs.

Although numerous peaks are observed, the principal peaks seen in brain tumor MRS at 1.5 T include branch chain amino acids (0.9–1.0 ppm), lipid (0.9–1.5 ppm), lactate (1.3 ppm), alanine (1.5 ppm), *n*-acetyl aspartate (NAA; 2.0 ppm), choline (3.2 ppm), creatine (3.0 ppm and 3.9 ppm), and myoinositol (3.6 ppm). Note that creatine produces two resonant peaks because it contains two chemically nonequivalent species of protons, and that the lipid and amino acid peaks are broad because each contains a large

number of different molecules with numerous nonequivalent protons. For this reason, amino acids, lactate, and lipid peaks overlap. When distinction between these is critical, a combination of short and intermediate or intermediate and long echo time spectra can be used to distinguish these species based on phase cycling of their peaks with respect to NAA, creatine, and choline. NAA is a marker of neuronal number and function, creatine a marker of energy metabolism and stores, and choline a marker of membrane synthesis and degradation ("membrane turnover"). All processes that injure neurons decrease NAA; all processes that injure glia or stimulate glial division increase choline; all processes that disrupt aerobic glycolysis result in lactate formation; and all processes that produce necrosis release lipid and decrease creatine [52–54]. Because the normal concentrations of these metabolites vary by anatomic location and because the relative signal detected from a given concentration of each metabolite varies with echo time chosen for a spectroscopy sequence, reference to spectra of normal-appearing voxels is critical for clinical interpretation of MRS [55–59].

Magnetic resonance spectroscopy in differential diagnosis

Although the typical pattern of glioma spectra is well defined—high choline and low or absent NAA peaks, with lipid and lactate peaks often seen in GBM—studies of MRS for prediction of tumor histology have not shown sufficient specificity to make this a clinically useful adjunct in most cases. MRS of extra-axial tumors that do not arise from glial precursors, such as meningioma, generally reveal very high choline and no NAA because the tumors contain no neurons. Although the presence of a very high alanine peak in a subset of meningioma can be useful to suggest the diagnosis, a recent well-controlled study suggests that the presence of low levels of alanine detected in up to 80% of meningioma is not useful because it is detected in similar frequency in metastases and schwannoma [60]. This pattern may aid in the differentiation of large meningioma from peripheral-enhancing intra-axial neoplasms, particularly when MRS is used in combination with perfusion imaging (as described later), but has proved unreliable in the differentiation of metastases from GBM because both may show high choline, absent or very low NAA, and high lactate and lipid peaks.

Extensive investigation has failed to demonstrate that MRS adds value in differential diagnosis of tumor types or of tumor from non-neoplastic processes such as demyelination, ischemia, and gliosis [61–64]. The lack of specificity of the principal MRS markers explains this limitation. A large choline peak suggesting increased membrane turnover may be seen in neoplasia with rapid membrane formation and seen in demyelination or ischemia with rapid membrane breakdown. All three processes may injure neuronal function or integrity, reducing the NAA peak; ischemia and neoplasia may result in anaerobic metabolism and necrosis, producing lactate and lipid peaks. One notable exception to this rule is the distinction of abscess from

rim-enhancing tumor by demonstrating amino acids within the contents of the cyst, a finding that is essentially diagnostic of the presence of activated polymorphonuclear leukocytes, and thus of bacterial or, less likely, parasitic infection (Fig. 4) [5,65].

Magnetic resonance spectroscopy in preoperative glioma grading and operative guidance

Although MRS has not proved to be a reliable aid to tumor differential diagnosis, qualitative or quantitative detection of high choline/NAA peak height ratios has been shown in a number of studies to be predictive of the presence of high-grade tumor [19,66]. Similarly, the presence of lipid/lactate in untreated glioma suggests the presence of necrotic grade IV tumor [19,67]. Although there is considerable overlap between high-and low-grade tumor spectra, meticulously acquired spectra revealing choline/NAA ratios above 1.5 or analogous thresholds developed for choline/NAA ratios have been shown to improve the accuracy of anatomic MRI prediction of tumor grade [68–70]. Although more technically robust and cost-effective perfusion and permeability techniques have significantly reduced the use of MRS for

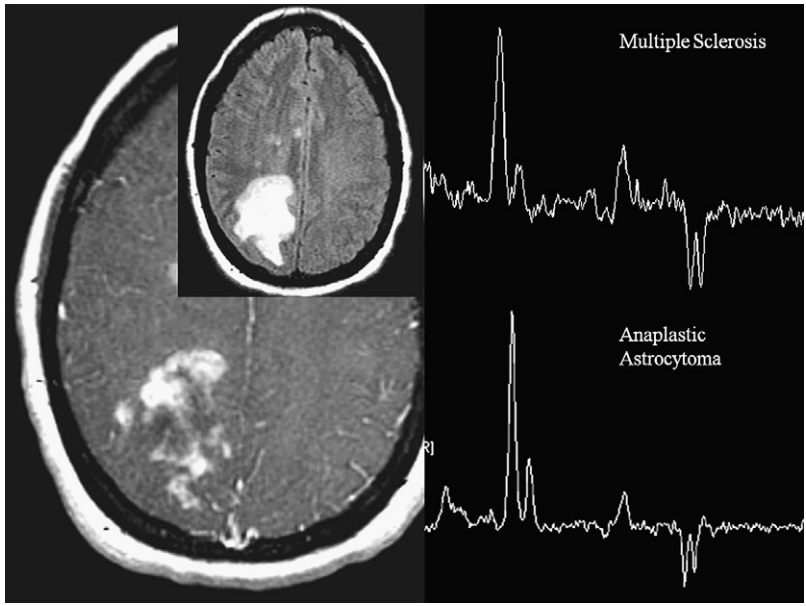

Fig. 4. Two spectra (echo time, 144 milliseconds) from patients who have heterogeneously enhancing white matter lesions. The indistinguishable spectra demonstrate elevated choline, low NAA, and moderate lactate. One spectrum represents tumefactive multiple sclerosis (MS); the other anaplastic astrocytoma. In anaplastic astrocytoma, choline elevation represents new membrane production, whereas in MS, it represents membrane injury. The patient whose images are shown in the top right spectrum turned out to have MS, but the comparison starkly illustrates the limitations of MR spectroscopy for differential diagnosis of new lesions.

tumor grade estimation, lesions suggestive of oligodendroglioma remain a notable exception because (as discussed later) high blood volume is seen even in low-grade oligodendroglioma, limiting the usefulness of perfusion for grading [71–74]. Also, some investigators have suggested that MRS may be especially useful compared with perfusion in patients in whom tumor recurrence is mixed with radiation necrosis, but this hypothesis is very difficult to prove because of the lack of appropriate gold standards [75].

The use of MRS to target biopsies to areas with high choline/NAA ratios has been reported to increase the accuracy of tumor biopsy by targeting areas of metabolically active tumor within areas of heterogeneous glioma, thus reducing the false-negative rate [76,77]. Similar methods have been used to guide stereotactic radiosurgery [78–80]. The true utility of MRS for these applications is difficult to assess with certainty because precise correlation of tissue pathology with anatomic location on MRI is difficult and the efficacy of surgical, radiosurgical, and focal ablative therapy is poor.

A recent report showed that glioma may decrease whole-brain NAA 30% more than can be explained by the visible tumor burden, suggesting that decreased whole-brain NAA may reflect the global burden of infiltrative tumor [81]. Because infiltration is a feature of glioma that cannot be detected reliably with current techniques, the significance of whole-brain NAA deserves further exploration as a marker of poor prognosis and diffuse tumor spread. Another recently reported MRS technique for detection of tumor infiltration that deserves further study is the use of CH_2/CH_3 ratios within the normal brain lipid pool to assay for tumor burden (Fig. 5) [82].

Magnetic resonance spectroscopy in assessment of treatment response

Because delayed radiation necrosis is also characterized by the presence of lactate/lipid peaks, the presence of these peaks alone is not useful in the distinction of radiation necrosis from tumor recurrence [83]. Complete absence of NAA and choline peaks or serial MRSI documenting progressive decrease in NAA and choline peaks combined with lactate/lipid peaks should suggest necrosis, particularly when corroborated by a rising ADC and low blood volume. Conversely, a significant increase in choline plus a decrease in NAA over time, with a consequent increase in the choline/NAA ratio or in derived statistics such as the choline/NAA ratio R value, is a sensitive indicator of tumor recurrence when seen in the appropriate anatomic imaging context [77,79,84–86]. Overall, serial MRSI under carefully controlled conditions has been shown to be a useful adjunct to conventional imaging for discrimination of high-grade focal brain tumor recurrence from delayed radiation necrosis in the hands of a few research groups, especially when combined with other imaging data. It is unfortunate that the spatial variation in choline, NAA, lactate, and lipid peaks within an individual tumor is often much greater than the change in these peaks over time. Thus, slight differences between scans in voxel placement or acquisition technique

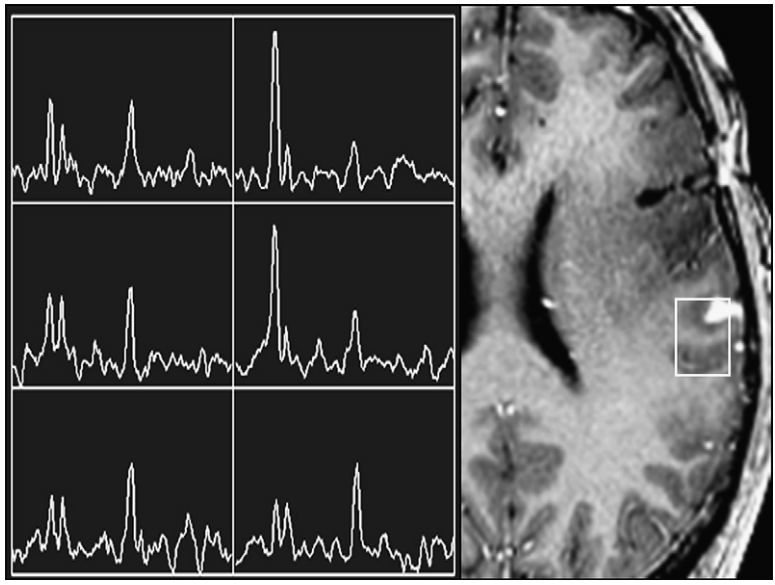

Fig. 5. 2D-MRSI demonstrates high choline/NAA ratio in two voxels within (*top row, middle column*) and immediately adjacent to (*middle row, middle column*) the area of abnormal enhancement, suggesting recurrent anaplastic astrocytoma. Other voxels demonstrate slightly increased choline/NAA ratio consistent with adjacent areas of lower-grade glioma. The rectangle overlayed on the right hand figure illustrates the anatomic location of the voxel from which the spectra were acquired.

can render the assessment of longitudinal change unreliable. Experience has shown that with currently available commercial MRI hardware and software, reliable clinical MRSI requires the direct supervision of each MRS data acquisition by a trained spectroscopist or supertechnologist under direct physician supervision. In the United States, where MRS and MRSI is not reimbursable at present, this requirement imposes a cost burden that has been impossible for most centers to meet and has prevented the establishment of serial MRSI brain tumor monitoring as a practical clinical tool at most centers.

Magnetic resonance spectroscopy summary

Selection of an appropriate area of interest and voxel size is critical to produce useful information while avoiding artifacts from partial volume averaging of calvarial marrow fat and susceptibility from bone or metal. Moreover, because the information provided by spectroscopy is generally not specific enough to be useful when only a single time point is available, serial comparison of change in spectra over time is critical for accurate interpretation. This need for serial comparison compounds the data acquisition problem because it requires a high degree of reproducibility in voxel selection over serial scans. As a result, the spectroscopy groups that have

had the greatest success using MRS and MRSI in neurooncology have found it necessary to develop significant additional human resources for monitoring data acquisition and processing beyond what is generally available in the routine clinical MR setting. At the present time, MRSI is not reimbursable, so the number of institutions with the financial resources to develop effective spectroscopy laboratories remains small, even among the major academic centers.

Microvascular imaging in brain tumor: perfusion-weighted imaging MRI and dynamic contrast-enhanced T1 permeability imaging

Much current basic biology research focuses on the interaction of tumor hypoxia, macrophage activation, and glioma gene expression in the transition from normal permeability and blood volume to increased native vessel permeability and volume and finally to frank neoangiogenesis during transformation from low-grade glioma to GBM [87]. In areas in which infiltrative and cellular glioma supplied by native vessels becomes hypoxic, secretion of vasoactive substances (including vascular endothelial growth factor [VEGF], interleukin 8 [IL-8], platelet-derived growth factor [PDGF], and epidermal growth factor receptor [EGFR]) by glioma and host immune cells induces the expression of aquaporins (especially AQP4) and suppresses the expression of endothelial tight junction proteins, resulting in varying degrees of impairment of the blood-brain barrier (BBB) [88]. In GBM, on the other hand, new formation of dense beds of characteristically tortuous and structurally abnormal ''corkscrew'' neocapillaries produces the extremely high local tissue blood volume. In these neocapillaries, deficiency or absence of basal lamina and pericytes and reduced endothelial expression of occludins and other cell surface proteins result in large endothelial gaps or fenestrations and leaky intercellular tight junctions that together produce the markedly increased capillary permeability [89,90]. These two central features of tumor neovasculature are the focus of the two types of microvascular imaging methods discussed later: dynamic susceptibility T2*-weighted ''perfusion'' (PMR) techniques used to estimate the volume of the neovascular capillary bed during the first pass of a contrast bolus, and dynamic enhancement T1-weighted ''permeability'' (T1P) techniques used to estimate impairment of the BBB by monitoring passage of the contrast into the extravascular space during the first pass and early recirculation phases.

Microvascular hemodynamic imaging: perfusion-weighted imaging MRI

PMR of brain tumors relies on a high pressure injection of a large contrast dose to produce a dynamic decrease in signal intensity on susceptibility (T2*)-weighted images acquired serially throughout the whole brain every 1 to 2 seconds during the injection. The signal change in each voxel is used to compute the relative cerebral blood volume (rCBV) of that voxel, which can then be

displayed as a color map or as a graph of the change in signal intensity in a given area over time (time-intensity curve [TIC]). Because clinically available techniques produce relative rather than quantitative blood volume maps, the blood volumes of normal-appearing white and gray matter are used as internal references for visual comparisons and for region-of-interest measurements [91,92]. This methodology works reasonably well, because normal gray matter CBV is approximately 2.7 times that of white matter, a value just above the diagnostic thresholds of 1.5 to 2.5 that have been reported to be most useful for distinguishing high-grade from low-grade glioma. In addition to inspecting the rCBV maps, a reliable interpretation requires inspection of the TIC to detect and account for magnetic susceptibility, motion, bolus timing, and other artifacts. The shape of the TIC provides a rough estimate of capillary permeability that can be very useful in differential diagnosis.

Perfusion-weighted imaging MRI in preoperative differential diagnosis of intracranial masses

The rough estimate of permeability derived from the shape of the TIC can provide important clues to the nature of the lesion. Microvessels within tumors of extra-axial and nonglial origin—meningioma, choroid plexus papilloma, metastases, lymphoma, and so forth—do not form a BBB, so a very large fraction of the bolus leaks into the extravascular space during the first pass [93–95]. Because glioma microvessels form a BBB that is impaired but not absent, the TIC returns significantly toward baseline in these tumors, although not as much as in normal brain. The difference between these patterns can contribute significantly to the discrimination of tumor types in cases of peripherally located enhancing tumors when the differential diagnosis includes meningioma and peripheral GBM, and in periventricular enhancing lesions when the differential diagnosis includes choroid plexus papillocarcinoma and GBM (Figs. 6 and 7).

In addition, PMR can aid in distinction of intracranial abscess from cystic glioma by demonstrating an rCBV lower than or equal to the surrounding white matter in abscess [6]. Although a number of reports document that metastases have a variable blood volume that is related to the vascularity of the primary tumor and a range that overlaps with GBM, it is unclear how applicable the data reported in these studies are to rCBV calculated with standard-spin echoplanar technique [96–98]. Thus, pending further study of rCBV in metastasis, PMR is not as useful as DWI and MRS for distinction of abscess from cystic metastasis. In a solitary intra-axial enhancing lesion, however, the combination of significant TIC return to baseline and high rCBV favors glioma. Conversely, low rCBV and very high first-pass contrast leak favors metastasis or lymphoma, especially when correlation with DWI demonstrates high cellularity [9,94]. Finally, if a circumscribed cortical or subcortical lesion has imaging features otherwise suggestive of a circumscribed low-grade glioma but has rCBV maps that demonstrate

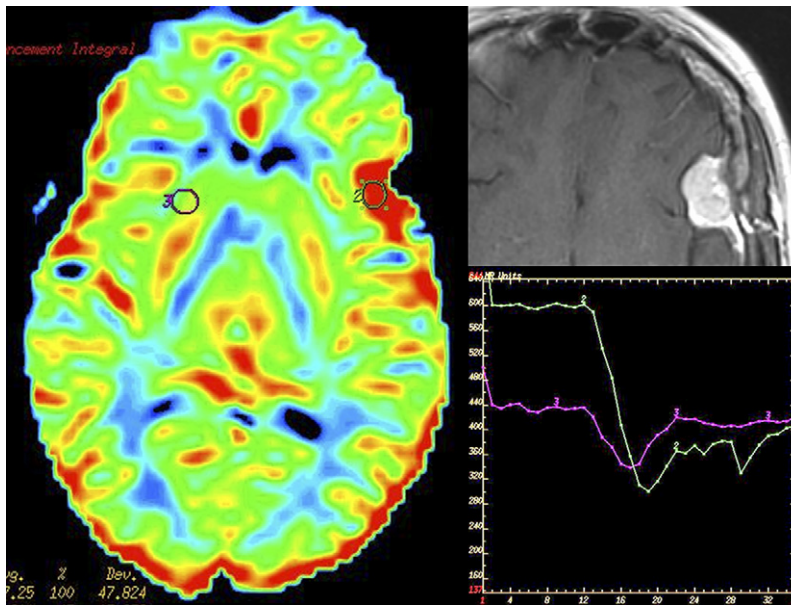

Fig. 6. PMR TIC (*lower right*) and rCBV map (*left*) demonstrate very high microvascular blood volume. The low return to baseline of the lesion TIC (*green curve*) compared with normal brain (*purple curve*) is characteristic of high first-pass leak in an extra-axial lesion without a BBB. In this case, the high permeability also produces prominent enhancement on the delayed post-Gd T1-weighted image (*upper right*) in a pattern strongly suggestive of meningioma, but the distinctive PMR findings illustrated can be very helpful in the differential diagnosis of less classic-appearing lesions.

prominent elevated blood volume equal or greater than cortical gray matter, then the diagnosis of oligodendroglioma should be suspected because the characteristic ''chicken-wire'' neocapillary architecture found in oligodendroglioma produces a high rCBV regardless of tumor grade. Although quantitative rCBV analysis may address this limitation in future, MRS remains important in these tumors (Fig. 8) [71–74].

Perfusion-weighted imaging MRI in preoperative tumor grade estimation

In known or suspected astrocytoma, the strong correlation between the maximum rCBV measured in a tumor and the histologic tumor grade has been extensively documented [99–105]. As noted earlier, the presence of tumor with an rCBV similar to or greater than cortex should strongly suggest the presence of grade IV tumor.

Perfusion-weighted imaging MRI in operative planning

Despite the limitations of low spatial resolution, susceptibility artifact, quantitation, and the difficulty of making longitudinal comparisons between

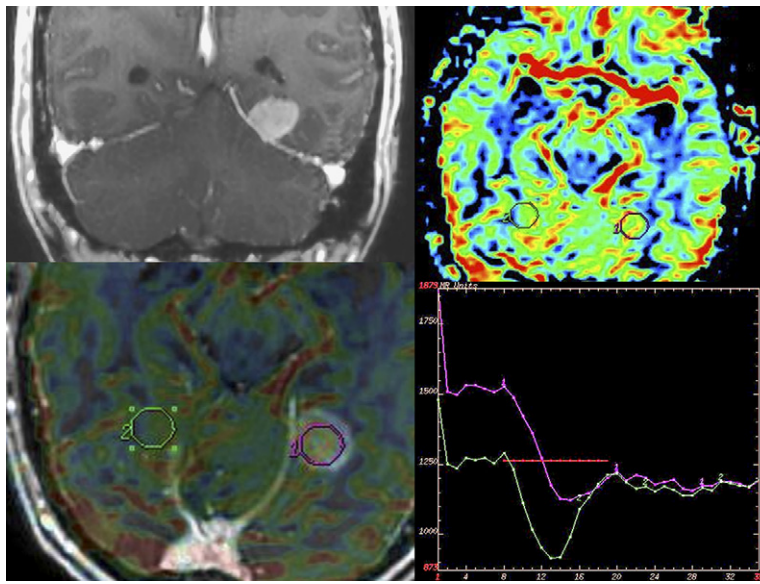

Fig. 7. Comparison of rCBV color map (*upper right*) and TIC (*lower right*) in regions of interest selected within the dural-based enhancing lesion (*lower left, purple*) and an appropriate region of interest in the contralateral white matter (*lower left, green*) demonstrate the characteristic high first-pass leak of a nonglial tumor (TIC) and blood volume only minimally higher than white matter (TIC and rCBV color map). In combination with the appearance on coronal post-Gd T1-weighted image (*upper left*), the perfusion imaging strongly suggests dural metastasis, confirmed at biopsy to be from non–small cell lung carcinoma.

echoplanar datasets, maximum rCBV has been demonstrated to be very helpful in preoperative planning to ensure biopsy, resection, or ablation of the highest-grade portion of a heterogeneous tumor [105–107].

Perfusion-weighted imaging MRI in follow-up of therapeutic response

Several well-designed studies have documented that low rCBV in combination with high ADC is typical of delayed radiation necrosis [28,108]. Early clinical experience using rCBV to detect tumor recurrence has been promising [109,110]. This application is especially interesting as we enter the age of antiangiogenic therapy because rCBV has been demonstrated to correlate with expression of angiogenic factors [102]. It is critical to obtain baseline preoperative rCBV maps to allow accurate interpretation of changing rCBV during follow-up, because the vascularity of glioma is very heterogeneous within a single patient's brain and between patients within a given tumor grade [106]. Correlation with steroid dosing during interpretation may be needed, although to date, technically rigorous reports looking at this subject have reached different conclusions as to whether high-dose steroid administration acutely reduces neovessel CBV in addition to its undisputed

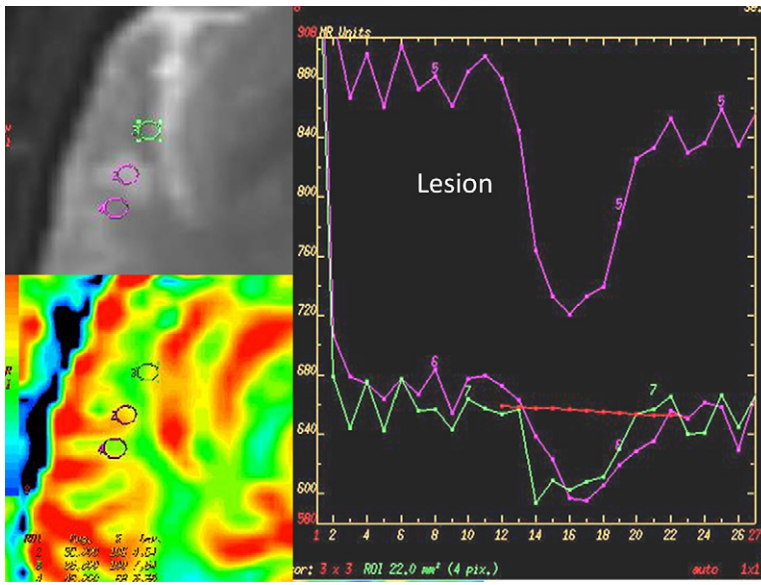

Fig. 8. TIC (*right*) and rCBV color map (*lower left*) demonstrating blood volume more than three times that of normal-appearing white matter in a small non-enhancing circumscribed lesion in the right temporal lobe suggest the diagnosis of oligodendroglioma. The upper TIC curve (*top left*) represents the lesion ROIs and the lower two curves the control ROIs.

effect on permeability [29,111,112]. This controversy will not be trivial to resolve definitively because alteration in permeability has a significant effect on the calculation of CBV (Fig. 9).

Microvascular permeability imaging: dynamic contrast-enhanced T1 permeability imaging

Low-grade astrocytomas supply their metabolic demand through co-optation of native brain capillaries and are thus limited in the rate of growth and bulk that they can achieve. Neoangiogenesis driven by autologous secretion of VEGF and other cytokines is one of the critical steps in the progression from lower-grade astrocytoma to anaplastic astrocytoma and GBM, enabling the rapid growth of solid tumor that conveys such poor prognosis. Cytokine-mediated abnormality of tight junctions in co-opted brain capillaries produces increased permeability to small molecules and electrolytes, which results in vasogenic edema in low- and high-grade glioma. In addition to permeable tight junctions, GBM neocapillaries have large endothelial gaps that produce a higher permeability to larger molecules, such as the Gd chelates used as MR contrast agents. The familiar enhancement of signal intensity on delayed T1-weighted images is a gross indicator of this abnormal permeability but has not proved to be a reliable

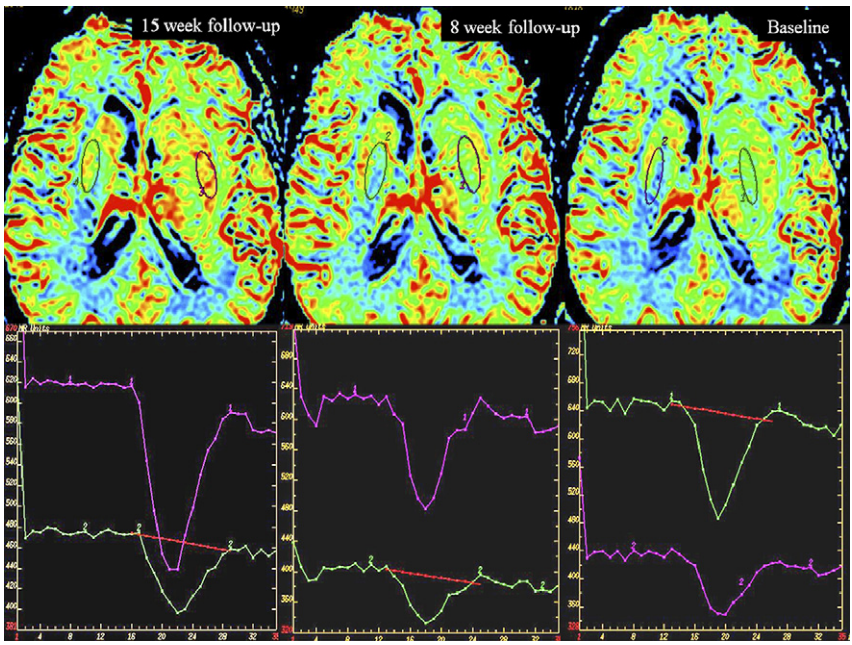

Fig. 9. Serial follow-up (*right to left*) rCBV maps (*top*) and TICs (*below*) demonstrate gradual but accelerating increase in blood volume within a left subinsular recurrent World Health Organization grade III to IV glioma. Although conventional imaging showed no significant change over the same interval, the 15-week follow-up perfusion region-of-interest data demonstrate definite extensive new hypervascularity 2.5 to 3.0 times that of contralateral basal ganglia, strongly suggestive of progressive high-grade recurrence.

predictor of tumor grade [1]. Because the pathophysiologic mechanisms contributing to abnormal permeability in GBM differ from those in lower-grade tumors, quantitation of the degree of abnormal permeability is a rational method of estimating the grade of tumor malignancy.

T1P is essentially a dynamic, semiquantitative adaptation of Gd-enhanced imaging, in which fast-gradient echo–based T1-weighted images of the whole brain continuously from before the contrast bolus arrival until 2 to 3 minutes after injection are used to measure the increase in signal intensity related to leakage of contrast agent from the intravascular compartment into the brain. Because of the lower temporal resolution and longer scan time, T1P is ideal for imaging the steady state leakage of contrast during the first few phases of bolus recirculation, in contrast to PMR, which images exclusively during the first pass. The TIC calculated from T1P can be used to derive a number of parameters related to BBB impairment, the most widely reported of which is the net forward volume transfer constant (K^{trans}) from the two-compartment pharmacokinetic modeling equation. Although K^{trans} is related to the slope of the delayed phase of the TIC, corrections for T2* effects, first-pass effects, flow, and surface area are necessary to

produce a true estimate. For this and other reasons, a number of different methods yielding related but distinct parameters such as the permeability surface area (K_{ps}) and forward transfer constant (K_1) are in use in different laboratories. Thus, the author refers to ''measures of permeability'' in the following text in recognition that most metrics reported in the literature are closely related but not necessarily equivalent to K^{trans}. Other metrics derived from T1P data currently under investigation, including relative recirculation [rR] histograms, are closely related to the maximum rate of enhancement during the first pass (max dI/dt), and may therefore reflect a somewhat different feature of microvessel architecture [113–116].

Dynamic contrast-enhanced T1 permeability imaging in preoperative estimation of tumor grade

As expected from the known correlation of neovessel abnormality with degree of malignancy in a number of models [89], the correlation of increased permeability with increasing tumor grade has been demonstrated to be robust, assuming that a reliable technique is used [113,115–118]. Reports that permeability measures are slightly less predictive of tumor grade than rCBV [118,119] come as no surprise because, in addition to neoangiogenesis, there are a large number of physiologic processes that may increase capillary permeability: local inflammatory response to the tumor, tumor ischemia, release of toxic metabolites, response to corticosteroids, use of immunosuppressant chemotherapeutic agents, and radiation injury, to name a few. As expected, although permeability is independent of blood volume [120], permeability measures are strongly correlated with rCBV in high-grade glioma [121], likely due to coregulation of neoangiogenesis and increased vascular permeability by VEGF and other proangiogenic factors. A large number of articles in press are exploring the utility of different combinations of blood volume and permeability metrics for improved tumor classification.

Dynamic contrast-enhanced T1 permeability imaging in postoperative therapeutic monitoring

Despite the large number of technique papers and early clinical demonstrations of T1P efficacy in distinction of tumor recurrence from necrosis [114,117], permeability measures have not yet achieved widespread clinical acceptance, largely because (1) the acquisition times are longer than for perfusion imaging, (2) the postprocessing is more complicated, (3) the plethora of metrics reported in the literature has yet to yield to a clear consensus metric, and consequently, (4) postprocessing algorithms in commercial release lag significantly behind perfusion software. Despite these shortcomings, the high sensitivity of T1P to antiangiogenic therapy is accelerating technique development. Future improvements in MR hardware and software

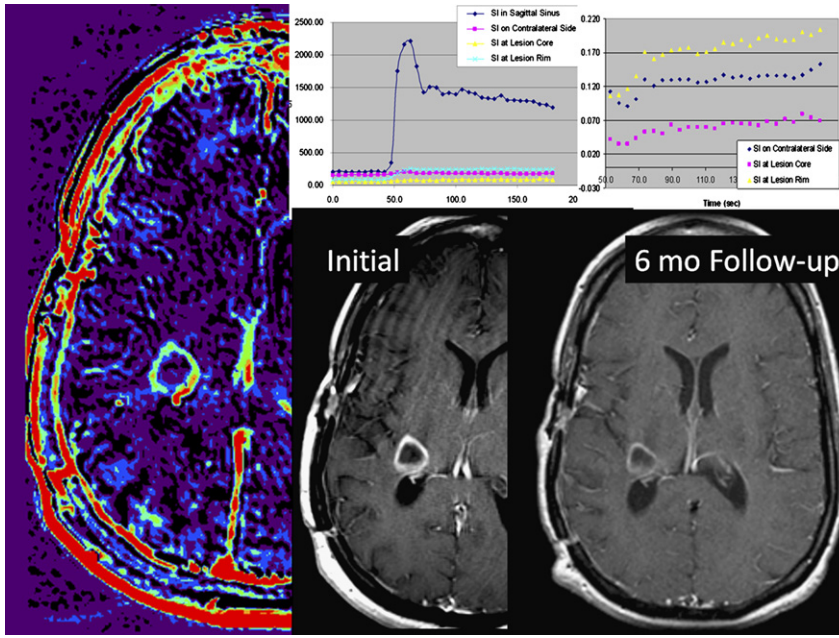

Fig. 10. Endothelial transfer constant (KPS) color map (*left*) and TICs pre and post normalization (*upper middle and upper right, respectively*) demonstrate only minimally increased permeability within the new ring-enhancing lesion (*lower middle*) in this patient post resection, radiation, and chemotherapy for gliosarcoma. The relatively mild increase in permeability suggested radiation necrosis rather than recurrence, as confirmed by the 6-month follow-up post-gadolinium T1-weighted image (*lower right*) showing no interval progression. (Postprocessing software courtesy of Timothy Roberts, PhD, Children's Hospital of Philadelphia.)

should allow acquisition at higher temporal and spatial resolutions and of more purely T1-weighted data. These advances, combined with an emergence of academic consensus and the development of standard commercial permeability postprocessing tools, may significantly alter clinical practice in this respect over the next few years (Figs. 10 and 11).

Summary

Advanced brain tumor MRI evaluation can now routinely produce an impressive array of in vivo data reflecting tumor cellularity, metabolism, invasiveness, neocapillary density, and permeability. Ongoing technical improvements and additional metrics, currently reported in the literature but too preliminary to review here, promise to bring to the clinic further dramatic increases in the quantity and quality of imaging data over the next 5 years. The clinical principles outlined in this article reflect only the most preliminary experience with these new data, but already it is becoming clear that a paradigm shift in neurooncology and neuropathology will be needed

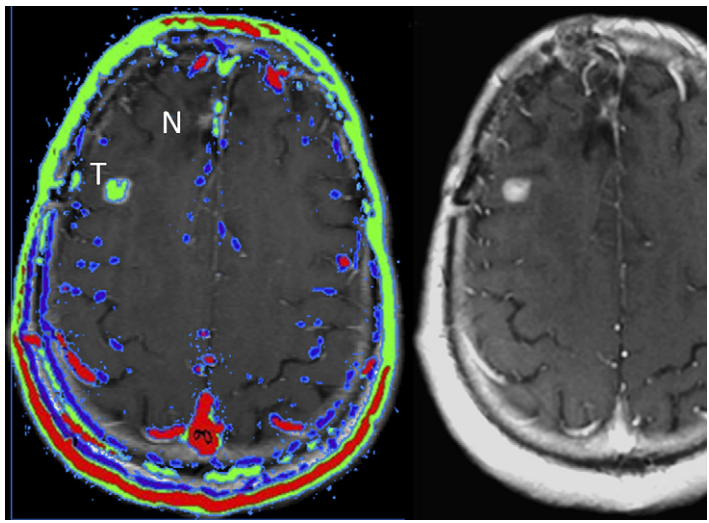

Fig. 11. Endothelial transfer constant (Kps) map superimposed on post-Gd spin-echo T-weighted image (*left*) in a patient who has a right frontal recurrent glioma shows focally elevated permeability similar to systemic scalp capillaries within the area of focal nodular enhancement (T), suggesting high-grade recurrence at this site but not in the area of enhancement at the anterior aspect of the right frontal resection site (N). Six-week follow-up post-Gd T1-weighted image (*right*) demonstrates interval decrease in enhancement at the anterior site (N) consistent with evolving necrosis, but not in the area of suspected recurrence. Although the potential utility of permeability data to aid in the differentiation of recurrent tumor from necrosis has been well established, clinical validation and routine application will require improvements in practicality and reproducibility. This type of data holds promise for distinguishing recurrent tumor from necrosis, but clinical validation and routine application await improvements in postprocessing and display technique. (Postprocessing software courtesy of Timothy Roberts, PhD, Children's Hospital of Philadelphia.)

if we are to make full use of the information available. The primary goal of neuropathologic glioma classification is to provide a clinically meaningful classification of brain tumors based on pathophysiology that will allow reliable prognosis and assessment of the efficacy of new therapies [122]. Already, the MRI data available (to say nothing of positron emission tomography and optical molecular imaging) reflect several independent aspects of brain tumor biology that cannot effectively be integrated into the existing histopathologic classification or used in treatment paradigms designed around that classification. Thus, although technical challenges remain, the greatest current challenge in advanced tumor imaging is the need for a new tumor classification method that can allow better integration of advanced imaging data into brain tumor research and clinical decision making. In essence, what is needed is a significant revision of brain tumor nosology. It is conceivable that a novel tumor classification method encompassing the new, advanced-MRI metrics in addition to nucleoside positron emission tomography data and cellular and molecular microarray data

could define novel pathophysiologically relevant subtypes that would better predict brain tumor patient prognoses and responses to targeted chemotherapeutic agents than our current histopathologic grading system. To this end, a number of recent reports have been published evaluating imaging markers by direct comparison with molecular genotype and phenotype [102] and patient outcomes [105,123]. This approach seems likely to become the dominant paradigm in the future.

References

[1] Ginsberg LE, Fuller GN, Hashmi M, et al. The significance of lack of MR contrast enhancement of supratentorial brain tumors in adults: histopathological evaluation of a series. Surg Neurol 1998;49(4):436–40.
[2] Provenzale J, Mukundan S, Barboriak DP. Diffusion-weighted and perfusion MR imaging for brain tumor characterization and assessment of treatment response. Radiology 2006; 239(3):632–49.
[3] Mardor Y, Pfeffer R, Spiegelmann R, et al. Early detection of response to radiation therapy in patients with brain malignancies using conventional and high b-value diffusion-weighted magnetic resonance imaging. J Clin Oncol 2003;21:1094–100.
[4] Reddy JS, Mishra AM, Behari S, et al. The role of diffusion-weighted imaging in the differential diagnosis of intracranial cystic mass lesions: a report of 147 lesions. Surg Neurol 2006;66(3):246–50.
[5] Mishra AM, Gupta RK, Jaggi RS, et al. Role of diffusion-weighted imaging and in vivo proton magnetic resonance spectroscopy in the differential diagnosis of ring-enhancing intracranial cystic mass lesions. J Comput Assist Tomogr 2004;28(4):540–7.
[6] Erdogan C, Hakyemez B, Yildirim N, et al. Brain abscess and cystic brain tumor: discrimination with dynamic susceptibility contrast perfusion-weighted MRI. J Comput Assist Tomogr 2005;29(5):663–7.
[7] Tsui EY, Leung WH, Chan JH, et al. Tumefactive demyelinating lesions by combined perfusion-weighted and diffusion weighted imaging. Comput Med Imaging Graph 2002;26(5): 343–6.
[8] Guo AC, Cummings TJ, Dash RC, et al. Lymphomas and high-grade astrocytomas: comparison of water diffusibility and histologic characteristics. Radiology 2002;224:177–83.
[9] Calli C, Kitis O, Yunten N, et al. Perfusion and diffusion MR imaging in enhancing malignant cerebral tumors. Eur J Radiol 2006;58(3):394–403.
[10] Okamoto K, Ito J, Ishikawa K, et al. Diffusion-weighted echo-planar MR imaging in differential diagnosis of brain tumors and tumor-like conditions. Eur Radiol 2000;10:1342–50.
[11] Toh CH, Chen YL, Hsieh TC, et al. Glioblastoma multiforme with diffusion-weighted magnetic resonance imaging characteristics mimicking primary lymphoma. Case report. J Neurosurg 2006;105:132–5.
[12] Krabbe K, Gideon P, Wagn P, et al. MR diffusion imaging of human intracranial tumours. Neuroradiology 1997;39(7):483–9.
[13] Kotsenas AL, Roth TC, Manness WK, et al. Abnormal diffusion-weighted MRI in medulloblastoma: does it reflect small cell histology? Pediatr Radiol 1999;29(7):524–6.
[14] Chenevert TL, Stegman LD, Taylor JM, et al. Diffusion magnetic resonance imaging: an early surrogate marker of therapeutic efficacy in brain tumors. J Natl Cancer Inst 2000; 92(24):2029–36.
[15] Chenevert TL, McKeever PE, Ross BD. Monitoring early response of experimental brain tumors to therapy using diffusion magnetic resonance imaging. Clin Cancer Res 1997;3(9): 1457–66.

[16] Filippi CG, Edgar MA, Ulug AM, et al. Appearance of meningiomas on diffusion-weighted images: correlating diffusion constants with histopathologic findings. AJNR Am J Neuroradiol 2001;22(1):65–72.
[17] Hayashida Y, Hirai T, Morishita S, et al. Diffusion-weighted imaging of metastatic brain tumors: comparison with histologic type and tumor cellularity. AJNR Am J Neuroradiol 2006;27(7):1419–25.
[18] Sugahara T, Korogi Y, Kochi M, et al. Usefulness of diffusion-weighted MRI with echo-planar technique in the evaluation of cellularity in gliomas. J Magn Reson Imaging 1999; 9:53–60.
[19] Catalaa I, Henry R, Dillon WP, et al. Perfusion, diffusion and spectroscopy values in newly diagnosed cerebral gliomas. NMR Biomed 2006;19(4):463–75.
[20] Yang D, Korogi Y, Sugahara T, et al. Cerebral gliomas: prospective comparison of multivoxel 2D chemical-shift imaging proton MR spectroscopy, echoplanar perfusion and diffusion-weighted MRI. Neuroradiology 2002;44:656–66.
[21] Bulakbasi N, Kocaoglu M, Ors F, et al. Combination of single-voxel proton MR spectroscopy and apparent diffusion coefficient calculation in the evaluation of common brain tumors. AJNR Am J Neuroradiol 2003;24:225–33.
[22] Castillo M, Smith JK, Kwock L, et al. Apparent diffusion coefficients in the evaluation of high-grade cerebral gliomas. AJNR Am J Neuroradiol 2001;22:60–4.
[23] Mardor Y, Roth Y, Ochershvilli A, et al. Pretreatment prediction of brain tumors' response to radiation therapy using high b-value diffusion-weighted MRI. Neoplasia 2004;6(2):136–42.
[24] Khan RB, Gutin PH, Rai SN, et al. Use of diffusion weighted magnetic resonance imaging in predicting early postoperative outcome of new neurological deficits after brain tumor resection. Neurosurgery 2006;59(1):60–6.
[25] Schaefer PW, Grant PE, Gonzalez RG. Diffusion-weighted MR imaging of the brain. Radiology 2000;217:331–45.
[26] Hein PA, Eskey CJ, Dunn JF, et al. Diffusion-weighted imaging in the follow-up of treated high-grade gliomas: tumor recurrence versus radiation injury. AJNR Am J Neuroradiol 2004;25:201–9.
[27] Chan YL, Yeung DK, Leung SF, et al. Diffusion-weighted magnetic resonance imaging in radiation-induced cerebral necrosis. Apparent diffusion coefficient in lesion components. J Comput Assist Tomogr 2003;27(5):674–80.
[28] Tsui EY, Chan JH, Ramsey RG, et al. Late temporal lobe necrosis in patients with nasopharyngeal carcinoma: evaluation with combined multi-section diffusion weighted and perfusion weighted MR imaging. Eur J Radiol 2001;39(3):133–8.
[29] Bastin ME, Carpenter TK, Armitage PA, et al. Effects of dexamethasone on cerebral perfusion and water diffusion in patients with high-grade glioma. AJNR Am J Neuroradiol 2006;27(2):402–8.
[30] Moffat BA, Chenevert TL, Lawrence TS, et al. Functional diffusion map: a noninvasive MRI biomarker for early stratification of clinical brain tumor response. Proc Natl Acad Sci U S A 2005;102(15):5524–9.
[31] Hamstra DA, Chenevert TL, Moffat BA, et al. Evaluation of the functional diffusion map as an early biomarker of time-to-progression and overall survival in high-grade glioma. Proc Natl Acad Sci U S A 2005;102(46):16759–64.
[32] Inoue T, Ogasawara K, Beppu T, et al. Diffusion tensor imaging for preoperative evaluation of tumor grade in gliomas. Clin Neurol Neurosurg 2005;107(3):174–80.
[33] Field AS, Wu YC, Alexander AL. Principal diffusion direction in peritumoral fiber tracts: color map patterns and directional statistics. Ann N Y Acad Sci 2005;1064: 193–201.
[34] Goebell E, Fiehler J, Ding XQ, et al. Disarrangement of fiber tracts and decline of neuronal density correlate in glioma patients—a combined diffusion tensor imaging and 1H-MR spectroscopy study. AJNR Am J Neuroradiol 2006;27(7):1426–31.

[35] Yu CS, Li KC, Xuan Y, et al. Diffusion tensor tractography in patients with cerebral tumors: a helpful technique for neurosurgical planning and postoperative assessment. Eur J Radiol 2005;56(2):197–204.
[36] Nimsky C, Grummich P, Sorensen AG, et al. Visualization of the pyramidal tract in glioma surgery by integrating diffusion tensor imaging in functional neuronavigation. Zentralbl Neurochir 2005;66(3):133–41.
[37] Lazar M, Alexander AL, Thottakara PJ, et al. White matter reorganization after surgical resection of brain tumors and vascular malformations. AJNR Am J Neuroradiol 2006; 27(6):1258–71.
[38] Schonberg T, Pianka P, Hendler T, et al. Characterization of displaced white matter by brain tumors using combined DTI and fMRI. Neuroimage 2006;30(4):1100–11.
[39] Provenzale JM, McGraw P, Mhatre P, et al. Peritumoral brain regions in gliomas and meningiomas: investigation with isotropic diffusion-weighted MR imaging and diffusion-tensor MR imaging. Radiology 2004;232(2):451–60.
[40] Price SJ, Burnet NG, Donovan T, et al. Diffusion tensor imaging of brain tumours at 3T: a potential tool for assessing white matter tract invasion? Clin Radiol 2003;58: 455–62.
[41] Lu S, Ahn D, Johnson G, et al. Peritumoral diffusion tensor imaging of high-grade gliomas and metastatic brain tumors. AJNR Am J Neuroradiol 2003;24:937–41.
[42] Lu S, Ahn D, Johnson G, et al. Diffusion-tensor MR imaging of intracranial neoplasia and associated peritumoral edema: introduction of the tumor infiltration index. Radiology 2004;232(1):221–8.
[43] Chiang IC, Kuo YT, Lu CY, et al. Distinction between high-grade gliomas and solitary metastases using peritumoral 3-T magnetic resonance spectroscopy, diffusion, and perfusion imagings. Neuroradiology 2004;46:619–27.
[44] Kono K, Inoue Y, Nakayama K, et al. The role of diffusion-weighted imaging in patients with brain tumors. AJNR Am J Neuroradiol 2001;22:1081–8.
[45] Stadnik TW, Chaskis C, Michotte A, et al. Diffusion-weighted MR imaging of intracerebral masses: comparison with conventional MR imaging and histologic findings. AJNR Am J Neuroradiol 2001;22:969–76.
[46] Sundgren PC, Fan X, Weybright P, et al. Differentiation of recurrent brain tumor versus radiation injury using diffusion tensor imaging in patients with new contrast-enhancing lesions. Magn Reson Imaging 2006;24(9):1131–42.
[47] Stieltjes B, Schluter M, Didinger B, et al. Diffusion tensor imaging in primary brain tumors: reproducible quantitative analysis of corpus callosum infiltration and contralateral involvement using a probabilistic mixture model. Neuroimage 2006;31(2):531–42.
[48] Zhou XJ, Engelhard HH, Leeds NE, et al. Studies of glioma infiltration using a fiber coherence index. Magn Reson Med, in press.
[49] van Westen D, Latt J, Englund E, et al. Tumor extension in high-grade gliomas assessed with diffusion magnetic resonance imaging: values and lesion-to-brain ratios of apparent diffusion coefficient and fractional anisotropy. Acta Radiol 2006;47(3):311–9.
[50] Marshall I, Wardlaw J, Cannon J, et al. Reproducibility of metabolite peak areas in 1H MRS of brain. Magn Reson Imaging 1996;14(3):281–92.
[51] Calvar JA. Accurate (1)H tumor spectra quantification from acquisitions without water suppression. Magn Reson Imaging 2006;24(9):1271–9.
[52] Birken DL, Oldendorf WH. *N*-acetyl-L-aspartic acid: a literature review of a compound prominent in 1H-NMR spectroscopic studies of brain. Neurosci Biobehav Rev 1989; 13(1):23–31.
[53] Moffett JR, Ross B, Arun P, et al. *N*-acetyl aspartate in the CNS: from neurodiagnostics to neurobiology. Prog Neurobiol 2007;81(2):89–131.
[54] Wyss M, Kaddurah-Daouk R. Creatine and creatinine metabolism. Physiol Rev 2000; 80(3):1107–213.

[55] Christiansen P, Toft P, Larsson HB, et al. The concentration of *N*-acetyl aspartate, creatine + phosphocreatine, and choline in different parts of the brain in adulthood and senium. Magn Reson Imaging 1993;11(6):799–806.
[56] Brief EE, Whittall KP, Li DK, et al. Proton T1 relaxation times of cerebral metabolites differ within and between regions of normal human brain. NMR Biomed 2003;16(8):503–9.
[57] Degaonkar MN, Pomper MG, Barker PB. Quantitative proton magnetic resonance spectroscopic imaging: regional variations in the corpus callosum and cortical gray matter. J Magn Reson Imaging 2005;22(2):175–9.
[58] Kent C. Regulatory enzymes of phosphatidylcholine biosynthesis: a personal perspective [review]. Biochim Biophys Acta 2005;1733(1):53–66.
[59] Babb SM, Ke Y, Lange N, et al. Oral choline increases choline metabolites in human brain. Psychiatry Res 2004;130(1):1–9.
[60] Cho YD, Choi GH, Lee SP, et al. (1)H-MRS metabolic patterns for distinguishing between meningiomas and other brain tumors. Magn Reson Imaging 2003;21(6):663–72.
[61] Gajewicz W, Papierz W, Szymczak W, et al. The use of proton MRS in the differential diagnosis of brain tumors and tumor like processes. Med Sci Monit 2003;9(9):MT97–T105.
[62] Preul MC, Caramanos Z, Collins DL, et al. Accurate, noninvasive diagnosis of human brain tumors by using proton magnetic resonance spectroscopy. Nat Med 1996;2:323–5.
[63] Del Sole A, Falini A, Ravasi L, et al. Anatomical and biochemical investigation of primary brain tumours [review]. Eur J Nucl Med 2001;28(12):1851–72.
[64] Delorme S, Weber MA. Applications of MRS in the evaluation of focal malignant brain lesions. Cancer Imaging 2006;22(6):95–9.
[65] Lai PH, Ho JT, Chen WL, et al. Brain abscess and necrotic brain tumor: discrimination with proton MR spectroscopy and diffusion-weighted imaging. AJNR Am J Neuroradiol 2002;23(8):1369–77.
[66] Devos A, Lukas L, Suykens JA, et al. Classification of brain tumours using short echo time 1H MR spectra. J Magn Reson 2004;170:164–75.
[67] Li X, Vigneron DB, Cha S, et al. Relationship of MR-derived lactate, mobile lipids, and relative blood volume for gliomas in vivo. AJNR Am J Neuroradiol 2005;26(4):760–9.
[68] Law M, Yang S, Wang H, et al. Glioma grading: sensitivity, specificity, and predictive values of perfusion MR imaging and proton MR spectroscopic imaging compared with conventional MR imaging. AJNR Am J Neuroradiol 2003;24(10):1989–98.
[69] Fayed N, Morales H, Modrego PJ, et al. Contrast/noise ratio on conventional MRI and choline/creatine ratio on proton MRI spectroscopy accurately discriminate low-grade from high-grade cerebral gliomas. Acad Radiol 2006;13(6):728–37.
[70] Chen J, Huang SL, Li T, et al. In vivo research in astrocytoma cell proliferation with 1H-magnetic resonance spectroscopy: correlation with histopathology and immunohistochemistry. Neuroradiology 2006;48(5):312–8.
[71] Jenkinson MD, Smith TS, Joyce K, et al. MRS of oligodendroglial tumors: correlation with histopathology and genetic subtypes. Neurology 2005;64(12):2085–9.
[72] White ML, Zhang Y, Kirby P, et al. Can tumor contrast enhancement be used as a criterion for differentiating tumor grades of oligodendrogliomas? AJNR Am J Neuroradiol 2005;26: 784–90.
[73] Lev MH, Ozsunar Y, Henson JW, et al. Glial tumor grading and outcome prediction using dynamic spin-echo MR susceptibility mapping compared with conventional contrast-enhanced MR: confounding effect of elevated rCBV of oligodendrogliomoas [sic]. AJNR Am J Neuroradiol 2004;25:214–21.
[74] Xu M, See SJ, Ng WH, et al. Comparison of magnetic resonance spectroscopy and perfusion-weighted imaging in presurgical grading of oligodendroglial tumors. Neurosurgery 2005;56:919–24.
[75] Chernov M, Hayashi M, Izawa M, et al. Differentiation of the radiation-induced necrosis and tumor recurrence after gamma knife radiosurgery for brain metastases: importance of multi-voxel proton MRS. Minim Invasive Neurosurg 2005;48(4):228–34.

[76] Gajewicz W, Grzelak P, Gorska-Chrzastek M, et al. [The usefulness of fused MRI and SPECT images for the voxel positioning in proton magnetic resonance spectroscopy and planning the biopsy of brain tumors: presentation of the method] [abstract]. Neurol Neurochir Pol 2006;40(4):284–90 [in Polish].
[77] Hall WA, Martin A, Liu H, et al. Improving diagnostic yield in brain biopsy: coupling spectroscopic targeting with real-time needle placement. J Magn Reson Imaging 2001;13(1):12–5.
[78] Payne GS, Leach MO. Applications of magnetic resonance spectroscopy in radiotherapy treatment planning. Br J Radiol 2006;79(Special Issue 1):S16–26.
[79] Graves EE, Nelson SJ, Vigneron DB, et al. A preliminary study of the prognostic value of 1H-spectroscopy in gamma knife radiosurgery of recurrent malignant gliomas. Neurosurgery (Baltimore) 2000;46:319–28.
[80] Graves EE, Pirzkall A, Nelson SJ, et al. Registration of magnetic resonance spectroscopic imaging to computed tomography for radiotherapy treatment planning. Med Phys 2001;28: 2489–96.
[81] Cohen BA, Knopp EA, Rusinek H, et al. Assessing global invasion of newly diagnosed glial tumors with whole-brain proton MR spectroscopy. AJNR Am J Neuroradiol 2005;26(9): 2170–7.
[82] Matulewicz L, Sokol M, Wydmanski J, et al. Could lipid CH2/CH3 analysis by in vivo 1H MRS help in differentiation of tumor recurrence and post-radiation effects? Folia Neuropathol 2006;44(2):116–24.
[83] Chan YL, Yeung DK, Leung SF, et al. Proton magnetic resonance spectroscopy of late delayed radiation-induced injury of the brain. J Magn Reson Imaging 1999; 10(2):130–7.
[84] Graves EE, Nelson SJ, Vigneron DB, et al. Serial proton MR spectroscopic imaging of recurrent malignant gliomas after gamma knife radiosurgery. AJNR Am J Neuroradiol 2001; 2:613–24.
[85] Plotkin M, Eisenacher J, Bruhn H, et al. 123I-IMT SPECT and 1H MR-spectroscopy at 3.0 T in the differential diagnosis of recurrent or residual gliomas: a comparative study. J Neurooncol 2004;70(1):49–58.
[86] Hollingworth W, Medina LS, Lenkinski RE, et al. A systematic literature review of magnetic resonance spectroscopy for the characterization of brain tumors [review]. AJNR Am J Neuroradiol 2006;27(7):1404–11.
[87] Kaur B, Tan C, Brat DJ, et al. Genetic and hypoxic regulation of angiogenesis in gliomas [review]. J Neurooncol 2004;70(2):229–43.
[88] Manoonkitiwongsa PS, Schultz RL, Whitter EF, et al. Contraindications of VEGF-based therapeutic angiogenesis: effects on macrophage density and histology of normal and ischemic brains. Vascul Pharmacol 2006;44(5):316–25.
[89] Liebner S, Fischmann A, Rascher G, et al. Claudin-1 and claudin-5 expression and tight junction morphology are altered in blood vessels of human glioblastoma multiforme. Acta Neuropathol (Berl) 2000;100(3):323–31.
[90] Davies DC. Blood-brain barrier breakdown in septic encephalopathy and brain tumours [review]. J Anat 2002;200(6):639–46.
[91] Nakagawa T, Tanaka R, Takeuchi S, et al. Haemodynamic evaluation of cerebral gliomas using XeCT. Acta Neurochir (Wien) 1998;140(3):223–33.
[92] Muizelaar JP, Fatouros PP, Schroder ML. A new method for quantitative regional cerebral blood volume measurements using computed tomography. Stroke 1997;28(10): 1998–2005.
[93] Yang S, Law M, Zagzag D. Dynamic contrast-enhanced perfusion MR imaging measurements of endothelial permeability: differentiation between atypical and typical meningiomas. AJNR Am J Neuroradiol 2003;24:1554–9.
[94] Hartmann M, Heiland S, Harting I, et al. Distinguishing of primary cerebral lymphoma from high-grade gliomas with perfusion-weighted magnetic resonance imaging. Neurosci Lett 2003;338:119–22.

[95] Rollin N, Guyotat J, Streichenberger N, et al. Clinical relevance of diffusion and perfusion magnetic resonance imaging in assessing intra-axial brain tumors. Neuroradiology 2006; 48(3):150–9.
[96] Essig M, Waschkies M, Wenz F, et al. Assessment of brain metastases with dynamic susceptibility-weighted contrast-enhanced MR imaging: initial results. Radiology 2003;228(1): 193–9.
[97] Kremer S, Grand S, Berger F, et al. Dynamic contrast-enhanced MRI: differentiating melanoma and renal carcinoma metastases from high-grade astrocytomas and other metastases. Neuroradiology 2003;45(1):44–9.
[98] Kremer S, Grand S, Remy C, et al. Contribution of dynamic contrast MR imaging to the differentiation between dural metastasis and meningioma. Neuroradiology 2004;46(8):642–8.
[99] Hakyemez B, Erdogan C, Ercan I, et al. High-grade and low-grade gliomas: differentiation by using perfusion MR imaging. Clin Radiol 2005;60(4):493–502.
[100] Knopp EA, Cha S, Johnson G, et al. Glial neoplasms: dynamic contrast-enhanced T2*-weighted MR imaging. Radiology 1999;211:791–8.
[101] Sugahara T, Korogi Y, Kochi M, et al. Correlation of MR imaging-determined cerebral blood volume maps with histologic and angiographic determination of vascularity of gliomas. AJR Am J Roentgenol 1998;171:1479–86.
[102] Maia AC, Malheiros SM, da Rocha AJ, et al. MR cerebral blood volume maps correlated with vascular endothelial growth factor expression and tumor grade in nonenhancing gliomas. AJNR Am J Neuroradiol 2005;26(4):777–83.
[103] Shin JH, Lee HK, Kwun BD, et al. Using relative cerebral blood flow and volume to evaluate the histopathologic grade of cerebral gliomas: preliminary results. AJR Am J Roentgenol 2002;179(3):783–9.
[104] Aronen HJ, Gazit IE, Louis DN, et al. Cerebral blood volume maps of gliomas: comparison with tumor grade and histologic findings. Radiology 1994;191(1):41–51.
[105] Chaskis C, Stadnik T, Michotte A, et al. Prognostic value of perfusion-weighted imaging in brain glioma: a prospective study. Acta Neurochir (Wien) 2006;148(3):277–85 [comment: 285].
[106] Lupo JM, Cha S, Chang SM, et al. Dynamic susceptibility-weighted perfusion imaging of high-grade gliomas: characterization of spatial heterogeneity. AJNR Am J Neuroradiol 2005;26(6):1446–54.
[107] Maia AC, Malheiros SM, da Rocha AJ, et al. Stereotactic biopsy guidance in adults with supratentorial nonenhancing gliomas: role of perfusion-weighted magnetic resonance imaging. J Neurosurg 2004;101(6):970–6.
[108] Tsui EY, Chan JH, Leung TW, et al. Radionecrosis of the temporal lobe: dynamic susceptibility contrast MRI. Neuroradiology 2000;42(2):149–52.
[109] Siegal T, Rubinstein R, Tzuk-Shina T, et al. Utility of relative cerebral blood volume mapping derived from perfusion magnetic resonance imaging in the routine follow up of brain tumors. J Neurosurg 1997;86(1):22–7.
[110] Sugahara T, Korogi Y, Tomiguchi S, et al. Posttherapeutic intraaxial brain tumor: the value of perfusion-sensitive contrast-enhanced MR imaging for differentiating tumor recurrence from nonneoplastic contrast-enhancing tissue. AJNR Am J Neuroradiol 2000;21(5): 901–9.
[111] Ostergaard L, Hochberg FH, Rabinov JD, et al. Early changes measured by magnetic resonance imaging in cerebral blood flow, blood volume, and blood-brain barrier permeability following dexamethasone treatment in patients with brain tumors. J Neurosurg 1999;90(2): 300–5.
[112] Wilkinson ID, Jellineck DA, Levy D, et al. Dexamethasone and enhancing solitary cerebral mass lesions: alterations in perfusion and blood-tumor barrier kinetics shown by magnetic resonance imaging. Neurosurgery 2006;58(4):640–6.
[113] Roberts HC, Roberts TP, Ley S, et al. Quantitative estimation of microvascular permeability in human brain tumors: correlation of dynamic Gd-DTPA-enhanced MR imaging with histopathologic grading. Acad Radiol 2002;9(Suppl 1):S151–5.

[114] Hazle JD, Jackson EF, Schomer DF, et al. Dynamic imaging of intracranial lesions using fast spin-echo imaging: differentiation of brain tumors and treatment effects. J Magn Reson Imaging 1997;7(6):1084–93.
[115] Uematsu H, Maeda M, Sadato N, et al. Vascular permeability: quantitative measurement with double-echo dynamic MR imaging—theory and clinical application. Radiology 2000; 214:912–7.
[116] Roberts HC, Roberts TPL, Brasch RC, et al. Quantitative measurement of microvascular permeability in human brain tumors achieved using dynamic contrast-enhanced MR imaging: correlation with histologic grade. AJNR Am J Neuroradiol 2000;21:891–9.
[117] Provenzale JM, Wang GR, Brenner T, et al. Comparison of permeability in high-grade and low-grade brain tumors using dynamic susceptibility contrast MR imaging. AJR Am J Roentgenol 2002;178:711–6.
[118] Law M, Yang S, Babb JS, et al. Comparison of cerebral blood volume and vascular permeability from dynamic susceptibility contrast enhanced perfusion MR imaging with glioma grade. AJNR Am J Neuroradiol 2003;25:746–55.
[119] Law M, Young R, Babb J, et al. Comparing perfusion metrics obtained from a single compartment versus pharmacokinetic modeling methods using dynamic susceptibility contrast-enhanced perfusion MR imaging with glioma grade. AJNR Am J Neuroradiol 2006;27(9): 1975–82.
[120] Jackson A, Kassner A, Annesley-Williams D, et al. Abnormalities in the recirculation phase of contrast agent bolus passage in cerebral gliomas: comparison with relative blood volume and tumor grade. AJNR Am J Neuroradiol 2002;23(1):7–14.
[121] Provenzale JM, York G, Moya MG, et al. Correlation of relative permeability and relative cerebral blood volume in high-grade cerebral neoplasms. AJR Am J Roentgenol 2006; 187(4):1036–42.
[122] Preusser M, Haberler C, Hainfellner JA. Malignant glioma: neuropathology and neurobiology [review]. Wien Med Wochenschr 2006;156(11–12):332–7.
[123] Law M, Oh S, Babb JS, et al. Low-grade gliomas: dynamic susceptibility-weighted contrast-enhanced perfusion MR imaging—prediction of patient clinical response. Radiology 2006; 238(2):658–67.